PERGAMON

Journal of Atmospheric and Solar-Terrestrial Physics 60 (1998) 917–940

Journal of ATMOSPHERIC AND SOLAR-TERRESTRIAL PHYSICS

Simulations of high-altitude discharges initiated by runaway breakdown

R. Roussel-Dupré*, E. Symbalisty, Y. Taranenko, V. Yukhimuk

Space and Atmospheric Sciences Group, MS D466, Los Alamos National Laboratory, Los Alamos, NM 87545, U.S.A.

Received 1 March 1997; accepted 11 February 1998

Abstract

Detailed 2D hydrodynamic and quasi-electrostatic simulations of high-altitude discharges driven by runaway air breakdown are presented for four cases, corresponding to sprites initiated by positive cloud-to-ground lightning strikes in which 200 C of charge is neutralized at an altitude of 11.5 km in 10, 7, 5 and 3 ms. We find that the computed optical emissions agree well with low-light level camera images of sprites, both in terms of the overall intensity and spatial distribution of the emissions. Our results show the presence of blue emissions extending down to 40 km (blue tendrils) and red sprite tops extending from 50 to 77 km. Simulated spectra show that N_2 1st positive emissions dominate in the wavelength range from 550 to 850 nm, in good agreement with observations. Strong radio pulses with durations of ~ 300 μs and peak electric field amplitudes ranging from 20 to 75 V/m at an altitude of 80 km and an approximate distance from the discharge of 50 km were computed. The magnitude and duration of these pulses is sufficient to cause breakdown and heating of the lower ionosphere (80–95 km) and leads us to suggest that sprites may also launch the EMP responsible for the production of elves. The computed values for the γ-ray fluxes are in agreement with observations of γ-ray bursts of atmospheric origin and the peak secondary electron densities which we obtain are in good agreement with recent measurements of HF echoes at mesospheric heights and associated with lightning.

1. Introduction

The existence of high-altitude optical transients that occur over the tops of thunderstorms is now well documented (see e.g., Franz et al., 1990; Boeck et al., 1990; Winckler et al., 1993; Vaughan et al., 1992, 1993; Lyons and Williams, 1993; Sentman and Wescott, 1993; Lyons, 1994; Winckler et al., 1994; Wescott et al., 1995; Sentman et al., 1995; Boeck et al., 1995). Their association with high-altitude electrical discharges, first predicted by Wilson (1925, 1956), seems no longer to be in question. The only remaining issue is whether these events are glow discharges, 'streamers', breakdown caused by strong quasi-electrostatic fields, breakdown caused by strong electromagnetic pulses launched by cloud-to-ground or intracloud lightning, electrical breakdown of the air initiated by relativistic electrons (i.e. runaway air breakdown), or some combination of these various mechanisms. In this paper we examine the viability of the runaway breakdown mechanism for the production of sprites and elves, but first we proceed with a review of the existing observational database and a discussion of the strengths and weaknesses of competing theories.

The initial measurements of high-altitude optical transients prior to 1994 served to define the brightness, altitude range, morphology, and frequency of the events. More recent observations have yielded additional information on the duration, spectrum, energetics, and dimensions of these events and has led to identification of several types of associated phenomena including red sprites, blue jets, blue starters, and elves (Lyons, 1994; Winckler et al., 1994; Wescott et al., 1995; Sentman et al., 1995; Boeck et al., 1995; Rairden and Mende, 1995; Fukunishi et al., 1996; Lyons, 1996). Sprites tend to occur above the anvils of large mesoscale convective systems (Lyons, 1994) and to be correlated with strong positive ground strokes with peak currents in excess of ~ 100 kA (Boccippio et al., 1995). They are predominantly red in

* Corresponding author. Tel.: 001 505 667 9228; fax: 001 505 665 3681; e-mail: rroussel-dupre@lanl.gov

S1364-6826/98/$—See front matter
PII: S1364-6826(98)00028-5

color above 60 km altitude and can extend to 90 km in height. The region of maximum brightness lies in an altitude range 66–74 km, while faint tendrils may extend downward to 40–50 km where blue emissions dominate (Sentman et al., 1995). The lateral dimension of a sprite ranges from 5 to 50 km with the largest dimensions associated with clusters of sprites and its duration is typically several ms but can extend to 200 ms (cf, Winckler et al., 1994). In some cases several intensity maxima have been observed during a single event (cf, Winckler et al., 1994; Boeck et al., 1995). Typically, the brightest central part of a single sprite has a diameter of 2 km and an onset time to peak intensity of approximately 0.3 ms (Rairden and Mende, 1995). The maximum brightness across a video field as reported by Sentman et al. (1995) is roughly 600 kR while estimates of the corresponding total optical energy yield is 1–5 kJ per event. Spectral measurements of sprites (Mende et al., 1995; Hampton et al., 1996) clearly show that the red color is associated with the N_2 1P system, indicating electron impact excitation as the source of the emissions. While both of these papers have noted the absence of the N_2^+ Meinel system in their measurements, Armstrong et al. (1996) have shown that the Meinel band is quenched at the altitudes of peak sprite emission (see also Piper et al., 1985). In addition, Armstrong et al. (1996) present N_2^+ 1N λ 4278 photometer data associated with sprites at close range and argue that the lack of N_2^+ 1N emissions in the data of Mende et al. (1995) is probably a result of atmospheric extinction. Supporting photometer data of λ 4278 emissions were obtained by Suszcynsky et al. (1996) who also present the first blue imagery of a sprite observed from the ground. These results together with measurements of very low frequency (VLF) radio wave perturbations associated with sprites (Inan et al., 1995) indicate that these events are accompanied by strong, transient ionization or breakdown of the upper atmosphere. Sprites generally occur in clusters and have even been observed to 'dance' across the screen of a video display. Sprites in the latter configuration are often referred to as 'dancers'.

Recent attempts to account for elves and sprites have been based primarily on conventional breakdown of the air, either as a result of large amplitude (>hundreds of V/m at 70 km altitude or >tens of V/m at 100 km) electromagnetic pulses (EMP) launched by strong (producing currents in excess of tens to hundreds of kA) horizontal lightning strikes (Inan et al., 1991; Taranenko et al., 1993a, b; Milikh et al., 1995; Rowland et al., 1995; Inan et al., 1996; Sukhorukov et al., 1996) or as a result of quasi-static electric field changes caused by strong lightning strikes (Pasko et al., 1995; Pasko et al., 1996). Because EMP models produce enhanced electron heating and ionization of the air primarily at altitudes above 80 km where the electric field threshold for breakdown is sufficiently small and where the coupling to the background plasma is most efficient, these models are generally invoked to explain elves. Early theoretical papers (e.g. Inan et al., 1991; Taranenko et al., 1993a, b) modeled the interaction of EMP from conventional lightning with the lower ionosphere and established the major parameters of the perturbations for electron energy, electron density and emissions of light. In terms of optical emissions it was established that only strong lightning EMP with electric fields above 20 V/m are capable of producing optical flashes with an intensity above the background nighttime luminosity at 85–95 km altitudes (Taranenko et al., 1993b). The horizontal and vertical dimensions of the perturbed region as well as its altitude location coincide well with the experimental observations. Later computations by Rowland et al. (1995) and by Glukhov and Inan (1996) for an extended range of EMP parameters, and by Inan et al. (1996) for details of the two dimensional interaction, confirmed the range of optical intensities and electron density perturbations obtained by Taranenko et al. (1993a, b) for the corresponding EMP range.

The quasi-electrostatic models based on conventional breakdown extend to lower altitudes where emissions from sprites are observed, but must invoke large continuing currents and field enhancements around the initial high-altitude portion of the discharge in order to drive a propagating ionization channel to altitudes below 60 km. The introduction of an arbitrary recombination term for the purposes of numerical smoothing makes it difficult to assess the validity of these models. In addition, large amounts of charge ($\sim$200–475 C) must be neutralized in order to establish mesospheric fields above the conventional breakdown threshold. The advantages of quasi-electrostatic models based on runaway air breakdown are numerous. The threshold electric field needed to initiate this mechanism is a factor of ten less than that required for conventional breakdown. As a result, the runaway mechanism will proceed first under any electric field configuration that has sufficient scale lengths (tens to hundreds of meters) and will limit the strength of the driving electric field, thereby preventing conventional breakdown from proceeding. The amount of charge neutralization required is also substantially reduced for runaway. Depending on the initiating charge distribution, the runaway threshold can be exceeded throughout the atmosphere above the thundercloud and the ensuing discharge can therefore produce substantial emissions both at low altitudes where blue tendrils are observed as well as high altitudes ($\sim$65 km) where the head of the sprite is formed. Initial models based on runaway breakdown (Taranenko and Roussel-Dupré, 1996; Roussel-Dupré and Gurevich, 1996; Bell et al., 1995) show very good agreement with the gross features of sprites.

The occurrence of runaway discharges in and above thunderstorms is supported by a number of additional observations. Parks et al. (1981) and McCarthy and Parks (1985) have flown X-ray spectrometers through

thunderstorms at altitudes of 12 km and observed sharp enhancements in the X-ray flux from 3 to 110 keV just prior to a lightning strike. Bursts of intense, hard γ-ray emission from the atmosphere were observed by the Burst and Transient Signal Experiment (BATSE) aboard the Compton Gamma-ray Observatory (CGRO) when the subsatellite point was above large thunderstorm complexes near the equator (Fishman et al., 1994). In order to escape the atmosphere these γ-rays would have to originate above 25 km altitude. More recently Eack et al. (1996) measured strong X-ray pulses lasting approximately one second from a balloon at 15 km altitude above a mesoscale convective system. Only discharges initiated by the runaway mechanism could account for γ-ray bursts and such enhanced fluxes of X-rays.

The purpose of this communication is to present the results of a series of two dimensional, quasi-electrostatic simulations of high-altitude discharges initiated by runaway breakdown and to illustrate their close correspondence to the more recent and more detailed observations of sprites. As noted by Roussel-Dupré and Gurevich (1996), high-altitude runaway discharges can be a powerful source of radio bursts. In this paper we show that for certain initial conditions runaway discharges can launch radio pulses strong enough to cause enhanced heating and breakdown of the airglow layer at altitudes around 85 km. We propose then that intense sprites could themselves be the source of elves.

In our simulations a multifluid approach similar to that of Taranenko and Roussel-Dupré (1996, hereafter TR) is used to model the relativistic electrons, secondary electrons, and the positive and negative ions. The primary difference between this work and TR is that the runaway discharge is evolved self-consistently throughout the time during which charge neutralization (initiated by a cloud-to-ground or intracloud discharge) in the cloud occurs. The calculations are also carried out at much longer times, until the discharge itself or the background conductivity eliminates the fields. The electrostatic equations are solved in a different way, providing significant savings in computational time. We present calculations of the optical emissions, spectra, radio emissions for frequencies less than 1 MHz, and γ-rays. Several cases corresponding to different types of initiating lightning strikes are discussed and a direct comparison with observations is provided.

2. Simulations

2.1. Hydrodynamic equations

The mechanism of runaway air breakdown was first proposed by Gurevich et al. (1992). A detailed kinetic treatment that describes the temporal evolution of the electron distribution function in a uniform background electric field is presented in Roussel-Dupré et al. (1994). Spatial diffusion of the runaway electrons due to scattering was described in Gurevich et al. (1994). In the collision dominated regime the runaway breakdown mechanism can be characterized by two populations of electrons, namely, primaries or energetic (>10 keV) runaway electrons, and low energy secondaries (<100 eV). The secondary (low energy) electrons produced in the avalanche process are collision dominated and establish equilibrium distributions on time scales much shorter than the time for runaway breakdown. Their mean properties are defined by the local electric field E and pressure p (scaled in the usual way as E/p) and can be derived from the standard swarm parameters (Huxley and Crompton, 1974). Because we have included the avalanche rate for secondary electrons in our equation set, we note that conventional breakdown is also included in our analysis.

We now describe an extension of earlier work (TR) that allows us to predict the full temporal evolution of upper atmospheric discharges now known as red sprites. In the present formulation (contrary to TR), the positive and negative ions produced as a result of ionization and attachment are permitted to contribute to the total electrical current density and hence the evolution of the self-consistent fields. Because of their large densities at low altitudes, the ion contribution to the net current is important for slow discharges (hundreds of ms, a regime not addressed in TR) even though they do not move far from their creation point during the time of the simulation. As a result, the advection terms for the positive and negative ions are dropped from the continuity equations.

Thus, except for minor modifications, the hydrodynamic equations that we use in this paper to describe a runaway discharge are equivalent to that adopted by TR and can be written:

$$\frac{\partial n_p}{\partial t} = -\nabla\cdot n_p v_p + R_p n_p + \frac{F_c}{\lambda_{mfp}}, \tag{1}$$

$$\frac{\partial n_s}{\partial t} = -\nabla\cdot n_s v_s + R_s n_p - \alpha n_s + v_i n_s - \alpha_r n_+ n_s, \tag{2}$$

$$\frac{\partial n_-}{\partial t} = \alpha n_s - \alpha_l n_+ n_-, \tag{3}$$

$$\frac{\partial n_+}{\partial t} = R_s n_p + R_p n_p + v_i n_s - \alpha_l n_+ n_- - \alpha_r n_+ n_s, \tag{4}$$

$$J = e(n_{++} - n_- v_- - n_s v_s - n_p v_p), \tag{5}$$

$$\frac{\partial E}{\partial t} = -4\pi J + \frac{\partial E_L}{\partial t}, \tag{6}$$

where n_p is the density of primary electrons (high energy runaway electrons), n_s is the density of secondary electrons, n_+ is the density of positive ions, n_- is the density of negative ions, R_p is the production rate of runaway

electrons, v_p is the mean primary electron velocity, F_c is the flux of cosmic-ray produced high-energy electrons, $R_s = \varepsilon_p/\varepsilon_i R_p$ is the production rate of secondary electrons, $\varepsilon_i = 34$ eV is the energy loss per ion pair produced in air, v_s is the mean velocity of secondary electrons, α is the three-body attachment rate, α_R is the recombination rate, ν_i is the avalanche rate for low-energy electrons (ionization minus dissociative attachment), α_I is the ion recombination rate, v_+ and v_- are the positive and negative ion mobility velocities, respectively, E is the total self-consistent electric field and E_L is the field resulting from charge neutralization in the cloud, i.e. the normal lightning event that provides the driving field for the upper atmospheric discharge. The diffusion and detachment terms of TR were dropped because they are insignificant. The ion mobilities are approximated by:

$$\mu\left[\frac{m^2}{V_s}\right] \approx 2.27\times 10^{-4}\frac{\rho(z=0)}{\rho(z)}$$

where ρ is the neutral density of the air. The mean free path, λ_{mfp}, of high energy electrons with mean energy ε_p is well defined in terms of the energy loss formula of Bethe (1930) and Bethe and Ashkin (1953): $\lambda_{mfp} = \varepsilon_p/F_D$ where

$$F_D = \frac{4\pi Ze^4 N_m}{mc^2}\frac{\gamma^2}{\gamma^2-1}S(\gamma)$$

and where

$$S(\gamma) = \ln\left(\frac{mc^2}{I}\sqrt{(\gamma^2-1)(\gamma-1)/2}\right) - \frac{\ln(2)}{2}\left(\frac{2}{\gamma}-\frac{1}{\gamma^2}\right)+\frac{2}{2\gamma^2}+\frac{(\gamma-1)^2}{16\gamma^2}.$$

In the above equations we have $Z = 14.5$, N_m is the neutral air number density, m is the electron mass, e is the electron charge, and $I = 80.5$ eV. We also note that eqn (6) can be derived from Poisson's equation and the continuity equation in the electrostatic limit, and that it is more efficient computationally to solve because the current density is defined locally and the external lightning field is known analytically.

The parameters ε_p, v_p and R_p are available as a function of E/p from the detailed kinetic calculations for a limited number of values of E/p. These tabular data are fitted with smooth polynomials that are then used in the numerical simulations. Near an altitude of about 55 km the mean free path of the primary electrons becomes large and, in fact, comparable to an atmospheric scale height and to computational cell dimensions. A simple prescription is invoked to allow the primary electrons to free stream out the top of the computational grid. Because we are assuming a 2D cylindrically symmetric geometry, the free streaming primary electrons are given a vertical velocity component only. Their speed is adjusted to conserve kinetic energy. In reality, the electrons would be circulating around and moving in the direction of the geomagnetic field. We note that this effect does not alter the results of our model of the discharge because in runaway breakdown the energetic electrons escape in energy as well and do not alter their velocities significantly. In addition, detailed kinetic calculations show that the avalanche rate is determined entirely by the lower energy electrons near the threshold for runaway. These electrons are collision dominated and have smaller mean free paths. As a result the use of an avalanche rate based on the local value of E/p is completely justified. The reader is referred to Taranenko and Roussel-Dupré (1997) for a discussion of geomagnetic field effects. The free streaming model also allows us to estimate the flux of primary electrons to the ionosphere as a function of time. The continued evolution of the primary electron beam through the ionosphere along geomagnetic flux tubes is the subject of future research.

The parameters v_s, α, α_R, α_D, and ν_i are available as a function of E/p from the literature (e.g. Huxley and Crompton, 1974; Ali, 1986). Note that the associated primary and secondary electron conductivities can be obtained by dividing the corresponding currents by the electric field. These conductivities are evolved self-consistently in time (as are the currents) and include changes in electron energy through the parameterization of electron mobility (and/or drift velocity) in terms of E/p. The flux F_c of high-energy secondary electrons is also available from the literature (e.g. Daniel and Stephens, 1974) for energies greater than 10 MeV. We extend the energy down to 1 MeV by assuming that the distribution function, f, varies as: $f = f_0(\varepsilon_0/\rho)^{1.3}$ with the result that the integrated flux of electrons with energy above 1 MeV is given by:

$$F_c\left[\frac{\text{electrons}}{\text{cm}^2\text{s}}\right] \approx 2.5\, e^{-(H-11.2)/11.3}$$

where H is the altitude in km. Given that the electric field lies above the threshold for air-breakdown, then eqns (1)–(6) can be used to evolve the electron and ion densities as well as the electrostatic field vector E.

In thunderstorms, cloud electrification generally proceeds over a time scale (tens of seconds to tens of minutes) sufficiently long to permit the conducting atmosphere above the cloud to polarize and short out the thunderstorm electric field. When a lightning strike rapidly neutralizes the cloud charge layers (on time scales of ms to tens of ms), strong quasi-electrostatic fields can develop in the stratosphere and mesosphere. Given the background conductivity profile shown in Fig. 1, we can compute the resulting quasi-electrostatic fields that develop above the cloud for different charge con-

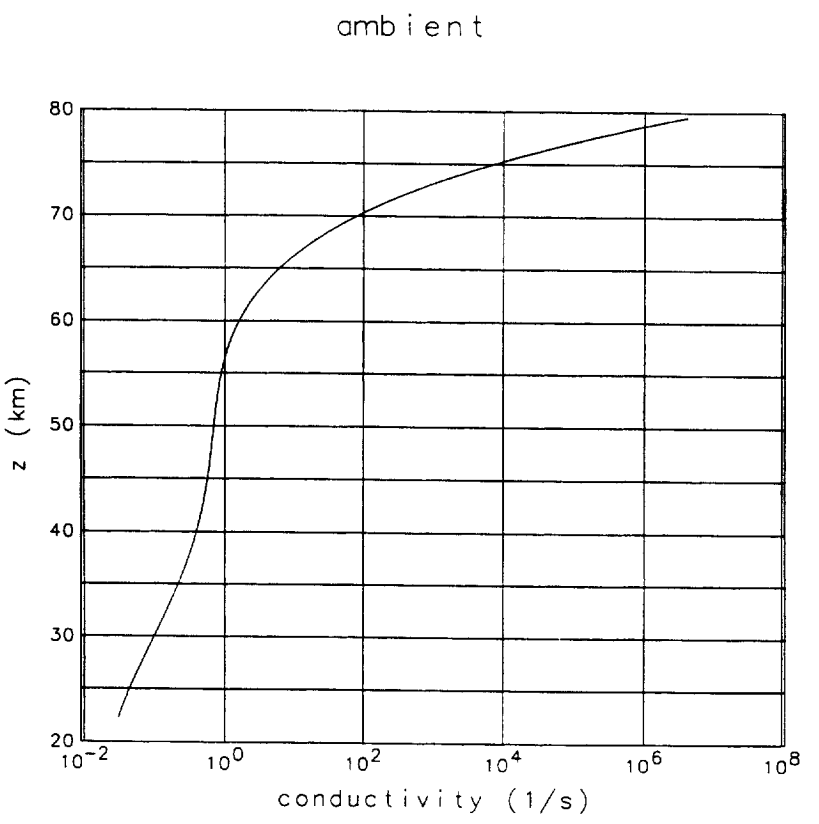

Fig. 1. Electrical conductivity profile. The electrical conductivity of the air (I/S) is plotted as a function of height.

figurations. Hence, the external, or normal lightning discharge field is found analytically. The positive cloud to ground strike in a storm complex is modeled by the creation of a monopole of opposite polarity in free air. The total charge, $-Q_{\text{discharge}}$, is created on an exponential time scale (τ) or via a constant current for a limited amount of time. For the exponential case, we have

$$Q(r,z,t) = Q(0,H,t) = -Q_{\text{discharge}}(1-e^{-t/\tau})$$

where H is the altitude of the discharge. For the case of an intracloud discharge in a storm complex the event is modeled as the creation of a dipole of opposite polarity in free air. The charges of opposite sign are now created at two altitudes with an exponential build up or with a constant current. This model neglects the complicated hydrodynamic and electrical processes within the storm complex and is therefore only valid well above the cloud tops. We have assumed that charge layers or charge centers can be approximated as point charges. Roussel-Dupré and Gurevich (1996) have solved for the electric field from these models, neglecting the resulting currents and charge distributions from the runaway process and neglecting the enhanced electrical conductivity due to the runaway process. This solution is useful for estimating the model parameters needed to produce different kinds of events. The solution for the dipole model of the intracloud discharge is reproduced here:

$$E_{\text{L}} = -\left[\frac{Q_{+}(\underline{r}-\underline{r}_{+})}{|\underline{r}-\underline{r}_{+}|^{3}} - \frac{Q(\underline{r}-\underline{r}_{-})}{|\underline{r}-\underline{r}_{-}|^{3}}\right]\frac{1}{1-4\pi\sigma\tau}[e^{-4\pi\sigma t}-e^{-t/\tau}], \tag{7}$$

where Q_{+} (Q_{-}) is the magnitude of the positive (negative) charge, $\underline{r}_{+}$ ($\underline{r}_{-}$) is the location of the positive (negative) charge layer, and σ is the background conductivity of the atmosphere. The image charges through a ground plane and an ionospheric plane (set at 100 km) are also included analytically in our analysis but not in eqn 7. We emphasize that eqn 7 was derived in the quasi-electrostatic limit (no radiation fields or propagation effects, i.e. the speed of light is effectively infinite) and assuming that the conductivity is constant with time. This equation is used only to estimate the parameters (Q and τ) necessary to initiate a runaway discharge. In the detailed numerical simulations, eqns 1–6 are solved self-consistently with the currents and associated conductivities determined from kinetic theory and/or swarm measurements par-

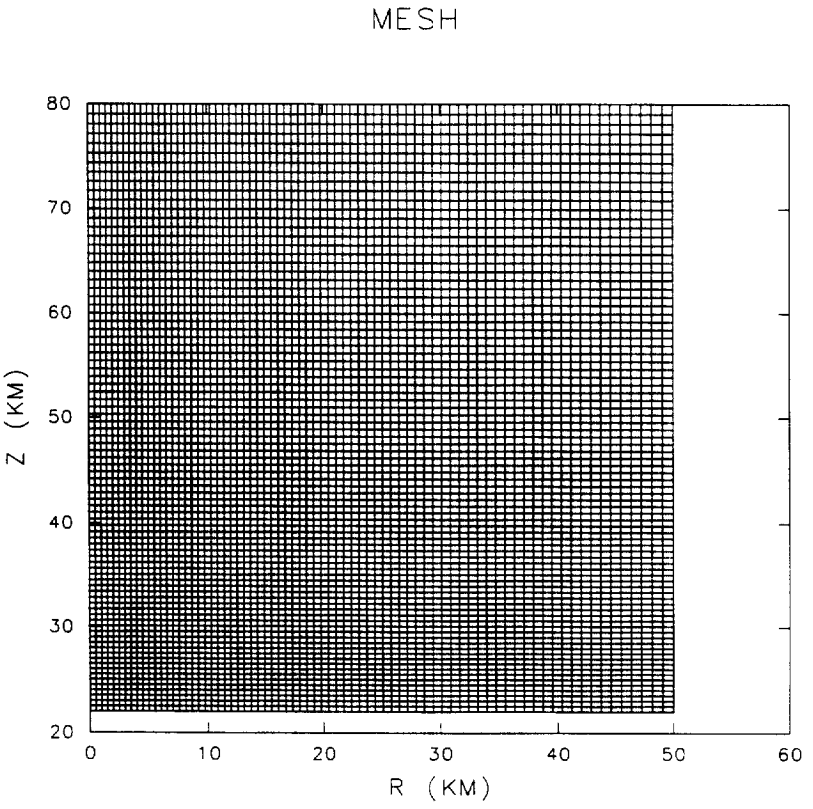

Fig. 2. Computational mesh. The cylindrical grid used in our simulations is shown. Note the variable spacing in both the radial and vertical directions.

ameterized as a function of E/p. Thus, changes in primary and secondary electron energies are incorporated into the conductivities which are also evolved self-consistently in time. The strength of the total electrical field, relative to the local threshold value for runaway breakdown to occur is defined as:

$$\underline{\delta}_0 = \underline{E}(r, z)/E_{\text{Threshold}}(z). \tag{8}$$

A transient, multimaterial, compressible, fluid dynamics code (CAVEAT) developed at Los Alamos (Adessio et al., 1992) was adapted to solve eqns (1)–(4) on a cylindrical grid with variable spacing as shown in Fig. 2. CAVEAT utilizes arbitrary mesh motion according to the 'arbitrary Langrangian-Eulerian' formulation. All of the simulations reported here were run in the pure Eulerian mode. A rectangular, but non-uniform, grid in r–z geometry is used in order to resolve the avalanche process at all altitudes. The avalanche length scales as $1/p$ and therefore increase exponentially in altitude. In our simulations there is square zoning near the left hand corner of the grid, typically 200–400 m. The radial and vertical grid spacings then increase at a constant factor (different in each direction) to reach the maximum radius and maximum height of the computational grid. Second order spatial differencing was employed along with explicit time marching. The independent state variables—densities and the electric field—are specified on cell centers. The derived velocity fields are cell centered. The advection terms in eqns (1) and (2) require face centered electron velocities which are computed from face centered electric fields. The face centered electric fields are computed from a simple average of the neighboring cell centered values.

The boundary conditions are described next. The electric field is set to zero above 80 km and therefore at the top boundary. The simulations are two dimensional with a left hand symmetry boundary. At this boundary the radial component of the electric field is set to zero, and the vertical component is set to the cell centered value next to the boundary. The bottom and right hand boundaries use the analytical expression for the electric field. On these two boundaries the time dependent conductivity of the neighboring real cell is used in the analytic expression. The primary and electron boundary velocities are derived from the electric field boundary values in the same way as the interior velocity distributions are determined. Outflow is allowed on the top and right hand boundaries, and outflow/inflow is allowed on the bottom boundary. The right hand boundary is chosen to be large

enough so that there is no significant avalanching near it and therefore the analytic electric field with the nearest real cell conductivity is appropriate. The bottom boundary is clearly an ad hoc situation. We have found that we must allow a current to flow across the boundary. In the case of no current flow an oscillating condition evolves where net charge near the bottom is allowed to build, which becomes large enough to attract opposite charge to neutralize it, which then allows it to build again and the cycle repeats. The combination of fine grid resolution, the analytic E field with nearest real cell conductivity, and the nearest real cell number densities in our estimation provide the most reasonable approximation to the actual current at this boundary.

The main effect of the runaway mechanism is to enhance the electrical conductivity greatly. This in turn affects the time evolution of the electric field through the dissipative current density term in eqn (6). Therefore we start our simulations just before the threshold for the runaway process is exceeded anywhere in the grid. At this problem-dependent, initial time the total and external electric fields are computed from eqn (7), i.e. the threshold for avalanching has not been reached anywhere and hence there is no runaway contribution to the fields. The simulation is ended when the maximum primary electron concentration is small, e.g. less than one per m^3. At this time the total electric field has been eliminated due to the enhanced electrical conductivity as well as the ambient electrical conductivity at high altitudes. The secondary electron populations persist to later times and in fact their existence may already be inferred from ground based radar echoes (Roussel-Dupré and Blanc, 1997) near and above thunderstorms.

2.2. Simulation results

The analytic expression for δ_0 allows us to search quickly the multi-dimensional parameter space of initiating lightning strokes. Figures 3(a)–(c) display snapshots in time of δ_0 for the case of -200 C discharged in an exponential time scale of 10 ms at an altitude of 11.5 km. This represents a positive cloud-to-ground stroke. Values greater than one, i.e. where the electric field exceeds the threshold for the relativistic avalanche to proceed, are color coded and values less than one are left white. We see that the avalanche first begins at high altitude (about 71 km) and moves downward encompassing the entire region from 22 km (the bottom of the grid) to 71 km. We have found, by numerical experiment, that the runaway region must extend down to about 35 km in order for the primary electron beam to traverse enough avalanche lengths to produce optical emissions strong enough to be detected by current low-light level cameras. Figure 3(d) displays the time evolution for the same case along the vertical axis of symmetry. The maximum value of δ_0 is 8.2 and therefore δ_0 lies below the threshold for conventional breakdown at any time along the z-axis. However, in the course of runaway breakdown there are two competing processes which can alter this result. The free streaming of primary electrons out of the discharge region will tend to increase the field while the enhanced conductivity associated with secondary electrons will tend to reduce it. In all the cases studied to date, we have found little or no contribution from conventional breakdown to the discharge.

We now describe results from four full simulations that reproduce the basic properties of red sprites. The initiating lightning strike is a positive cloud-to-ground stroke at 11.5 km altitude neutralizing 200 C. The exponential time scales are 10, 7, 5, and 3 ms for cases 1–4, respectively. Case 1 corresponds to the full detailed simulation of the analytical study described in the preceding paragraph. Case 2 represents a case that best matches visible observations of Sentman and Wescott (1993). Cases 3 and 4 allow us to study the effect of even smaller exponential time scales. The electron population morphology is quite similar for the four cases. There are several primary electron enhancements during the time evolution, but only three dominant, and optically visible, flashes. The first flash is an on axis beam [Fig. 4(a) for case 3] that flares radially [Fig. 4(b)] as it approaches the ionosphere. The second flash is spatially outside of the region of the first flash. It follows the first flash by 10, 6, 4, and 2 ms for cases 1–4, respectively. The third flash follows the second flash quite closely in time and is spatially at low altitude and outside the volume of the first two flashes. It is also much weaker. Note that the units in Figs. 4(a)–4(d) are in electrons/m, the color bars are identical for Figs 4(a) and 4(b), and also identical for Figs 4(c) and 4(d). The primary electron population dies rapidly after the third flash (see following paragraph). Figure 4(c) displays the secondary electron population at the same time (5.5 ms) as Fig. 4(a) for the primary electron population. Figure 4(d) displays the secondary population at 10 ms, for case 3, by which time the primary population has disappeared (i.e. less than 1/m).

Figure 5(a) displays the kinetic energy of the electron populations as a function of time for case 2. There are three peaks clearly visible for the primary electron population and each of these peaks corresponds to a flash of optical emissions. The first peak, as described above, is principally an on axis beam of electrons with a radius of 5–10 km. This beam eliminates the electric field within this region but the normal lightning stroke is still able to drive an avalanche around this region, about 5.5 ms later. This is the second peak in the kinetic energy plot. The third peak corresponds to a low altitude avalanche outside the first two regions in space. The primary beam abruptly shuts off at just over 14 ms because these three flashes have shorted out most of the spatial volume and the driving field (lightning stroke) is essentially over by 2τ. The peak kinetic energy of the secondary electron

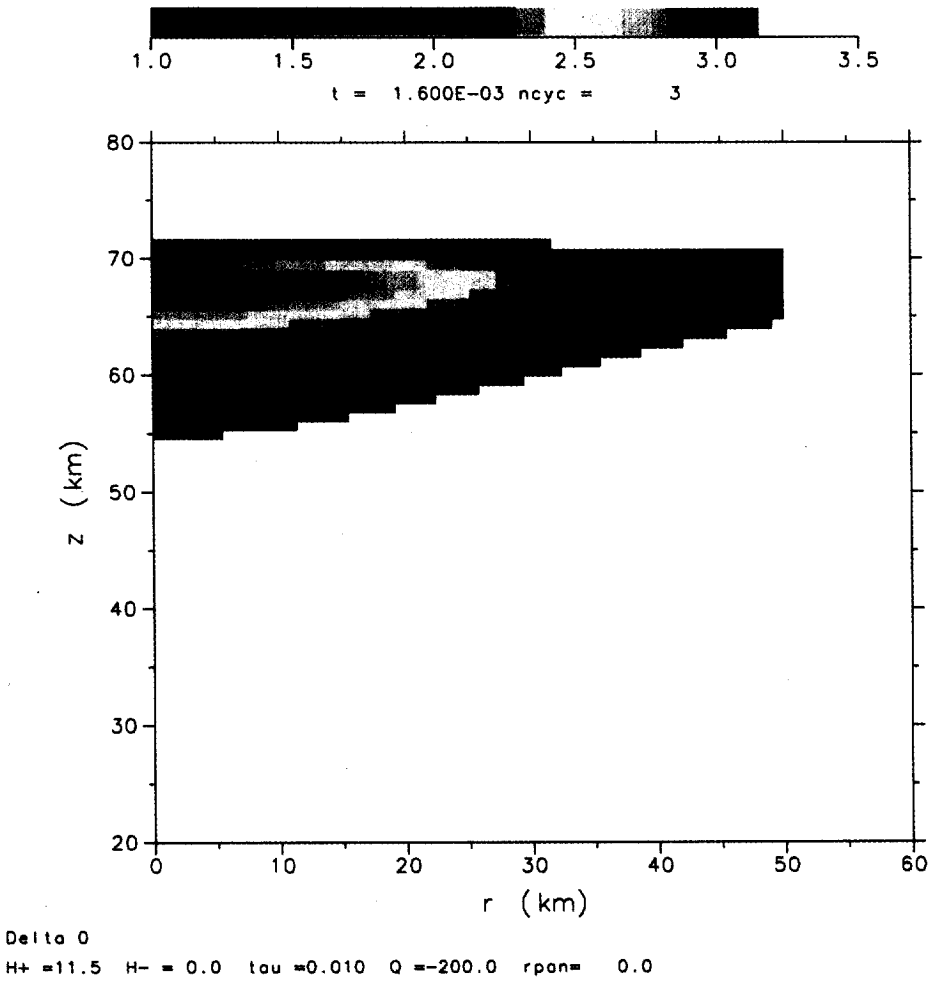

Fig. 3. Temporal evolution of δ_0. Two dimensional color contour plots showing the predicted magnitude of δ_0 produced by a positive cloud-to-ground lightning discharge are presented for Case 1 (neutralization of 200 C at 11.5 km altitude in 10 ms) at three times: (a) $t = 1.6$ ms, (b) $t = 10$ ms, and (c) $t = 30$ ms. The temporal evolution of δ_0 along the axis of the charge distribution in the cloud is shown in (d). Color bars for the magnitude of δ_0 are shown at the top of each plot. Values of δ_0 that are greater than one are color coded while those less than one are left blank.

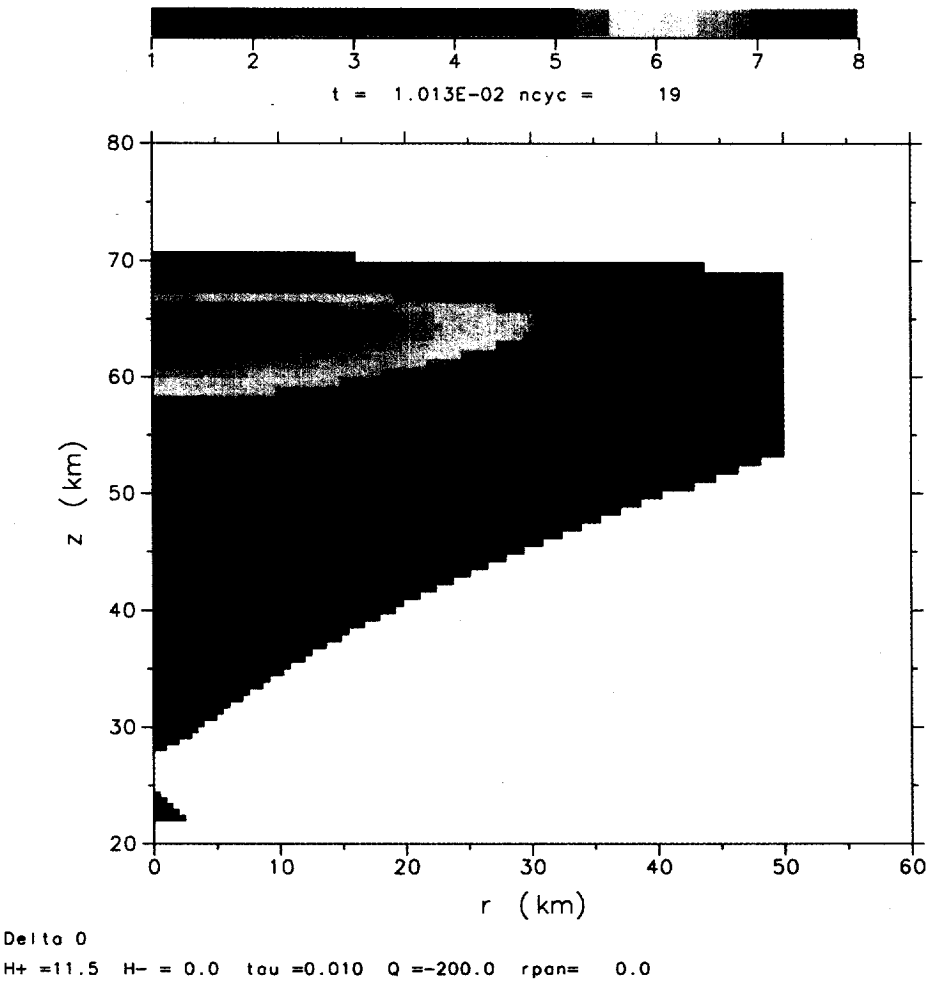
1
2
3
4
5
6
7
8
t = 1.013E-02 ncyc = 19
80
70
60
50
40
30
20
z (km)
0
10
20
30
40
50
60
r (km)
Delta 0
H+ =11.5 H- = 0.0 tau =0.010 Q =-200.0 rpan= 0.0

Fig. 3(b).

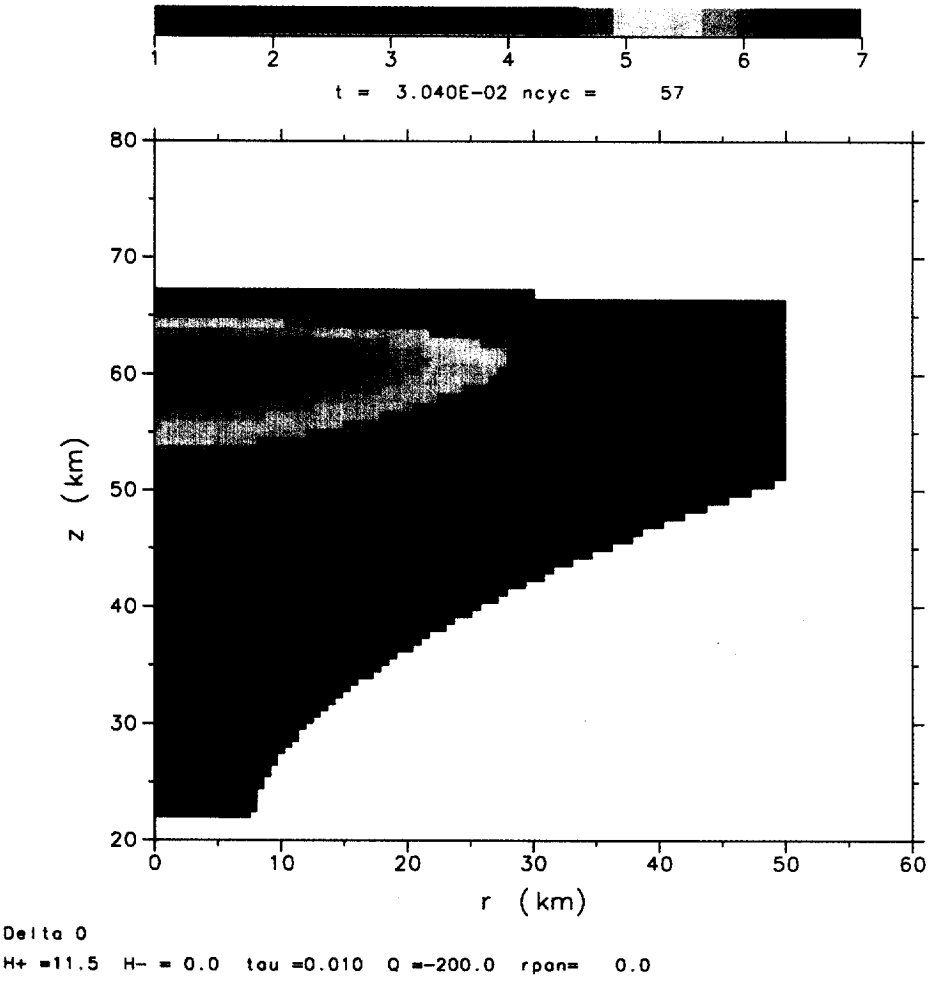
1
2
3
4
5
6
7
t = 3.040E-02 ncyc = 57
80
70
60
50
40
30
20
z (km)
0
10
20
30
40
50
60
r (km)
Delta 0
H+ =11.5 H- = 0.0 tau =0.010 Q =-200.0 rpan= 0.0

Fig. 3(c).

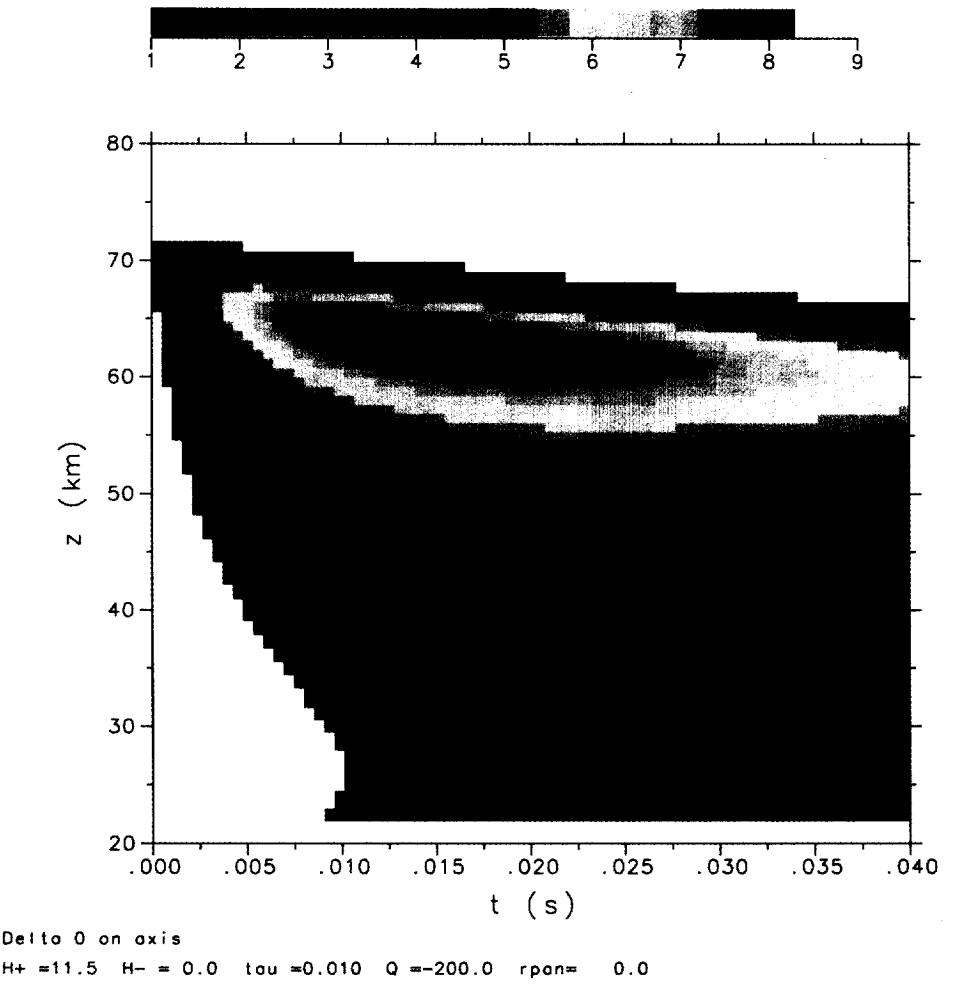
1
2
3
4
5
6
7
8
9
80
70
60
50
40
30
20
z (km)
.000
.005
.010
.015
.020
.025
.030
.035
.040
t (s)
Delta 0 on axis
H+ =11.5 H- = 0.0 tau =0.010 Q =-200.0 rpan= 0.0

Fig. 3(d).

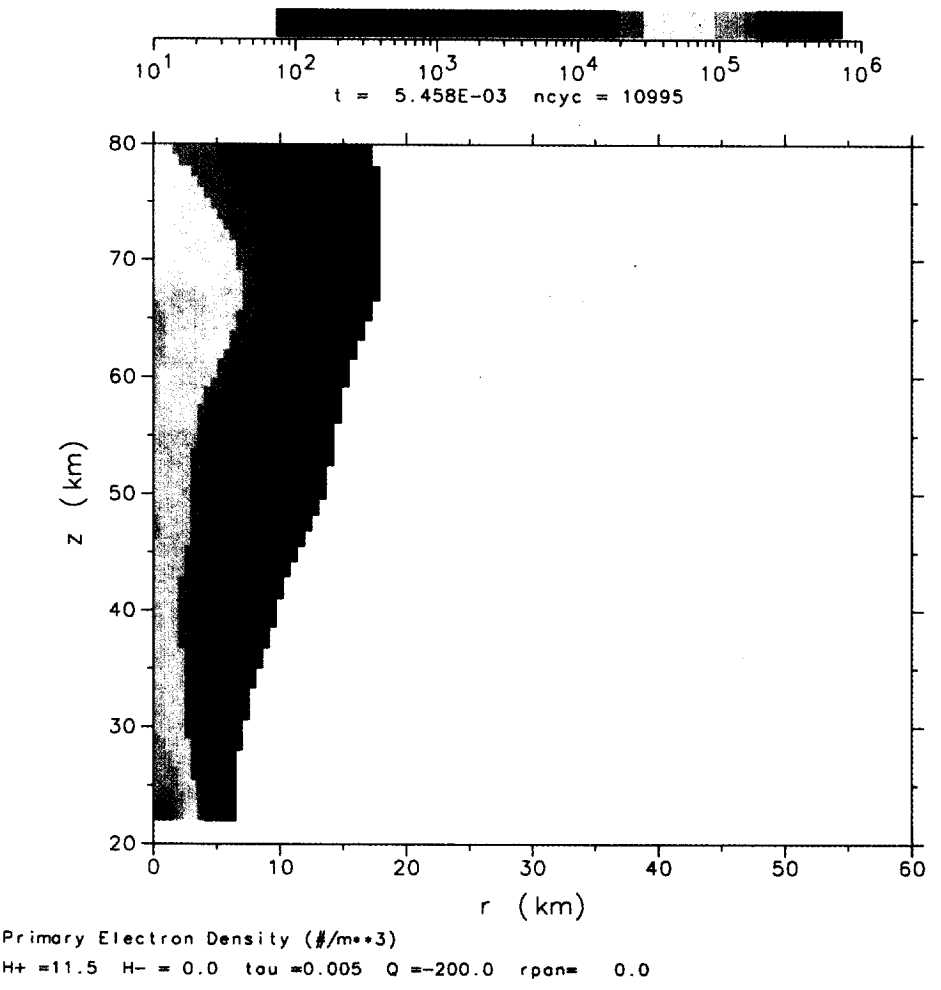

Fig. 4. Temporal evolution of primary and secondary electron densities. Two dimensional color contour plots showing the magnitude of the primary densities (in electrons/m^3) produced in a high-altitude runaway discharge initiated by a positive cloud-to-round lightning strike are presented for Case 3 (neutralization of 200 C at 11.5 km altitude in 5 ms) at two times: (a) $t = 5.46$ ms and (b) $t = 5.57$ ms. Similar plots for the secondary electron densities are presented for two times: (c) $t = 5.51$ ms and (d) $t = 10.4$ ms. Color bars for the magnitude of the densities are shown at the top of each plot. Densities that are less than the minimum color coded values (dark blue) in each plot are left blank.

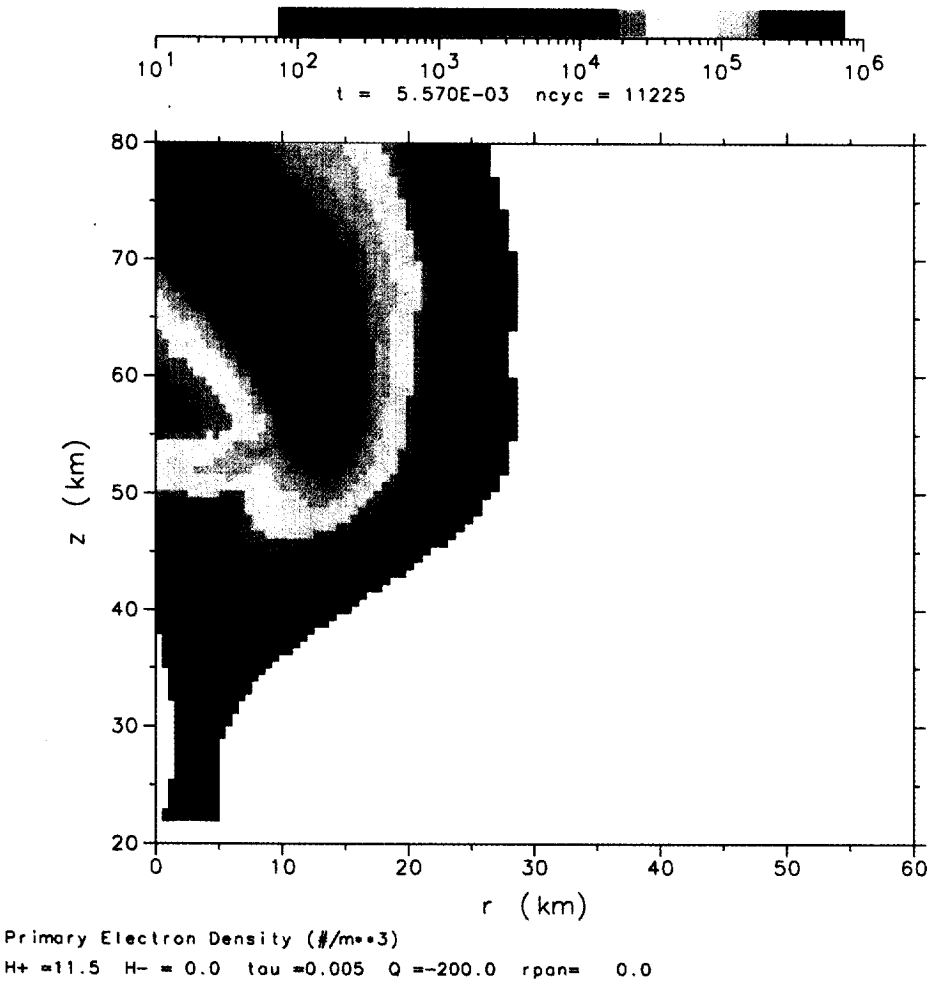
10^1
10^2
10^3
10^4
10^5
10^6
t = 5.570E-03 ncyc = 11225
80
70
60
50
40
30
20
z (km)
0
10
20
30
40
50
60
r (km)
Primary Electron Density (#/m**3)
H+ =11.5 H- = 0.0 tau =0.005 Q =-200.0 rpan= 0.0

Fig. 4(b).

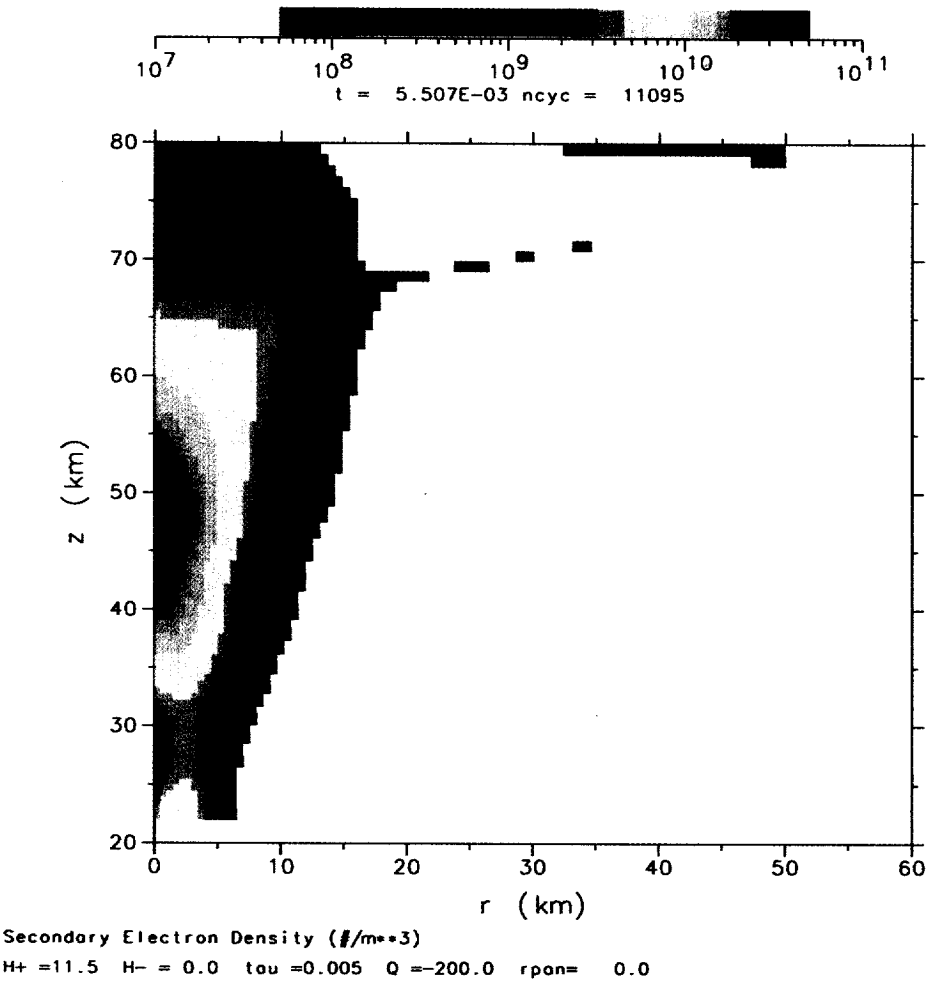
10^7
10^8
10^9
10^10
10^11
t = 5.507E-03 ncyc = 11095
80
70
60
50
40
30
20
z (km)
0
10
20
30
40
50
60
r (km)
Secondary Electron Density (#/m**3)
H+ =11.5 H- = 0.0 tau =0.005 Q =-200.0 rpan= 0.0

Fig. 4(c).

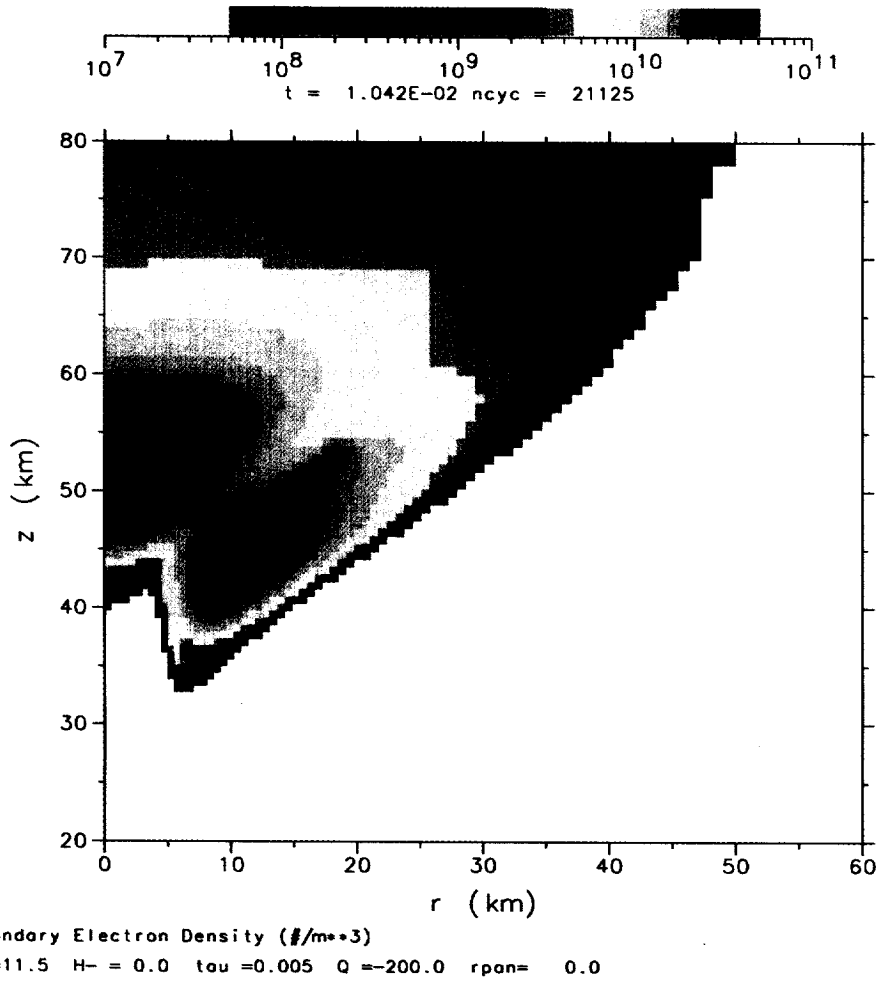
10^7
10^8
10^9
10^{10}
10^{11}
t = 1.042E-02 ncyc = 21125
80
70
60
50
40
30
20
z (km)
0
10
20
30
40
50
60
r (km)
Secondary Electron Density (#/m**3)
H+ =11.5 H- = 0.0 tau =0.005 Q =-200.0 rpan= 0.0

Fig. 4(d).

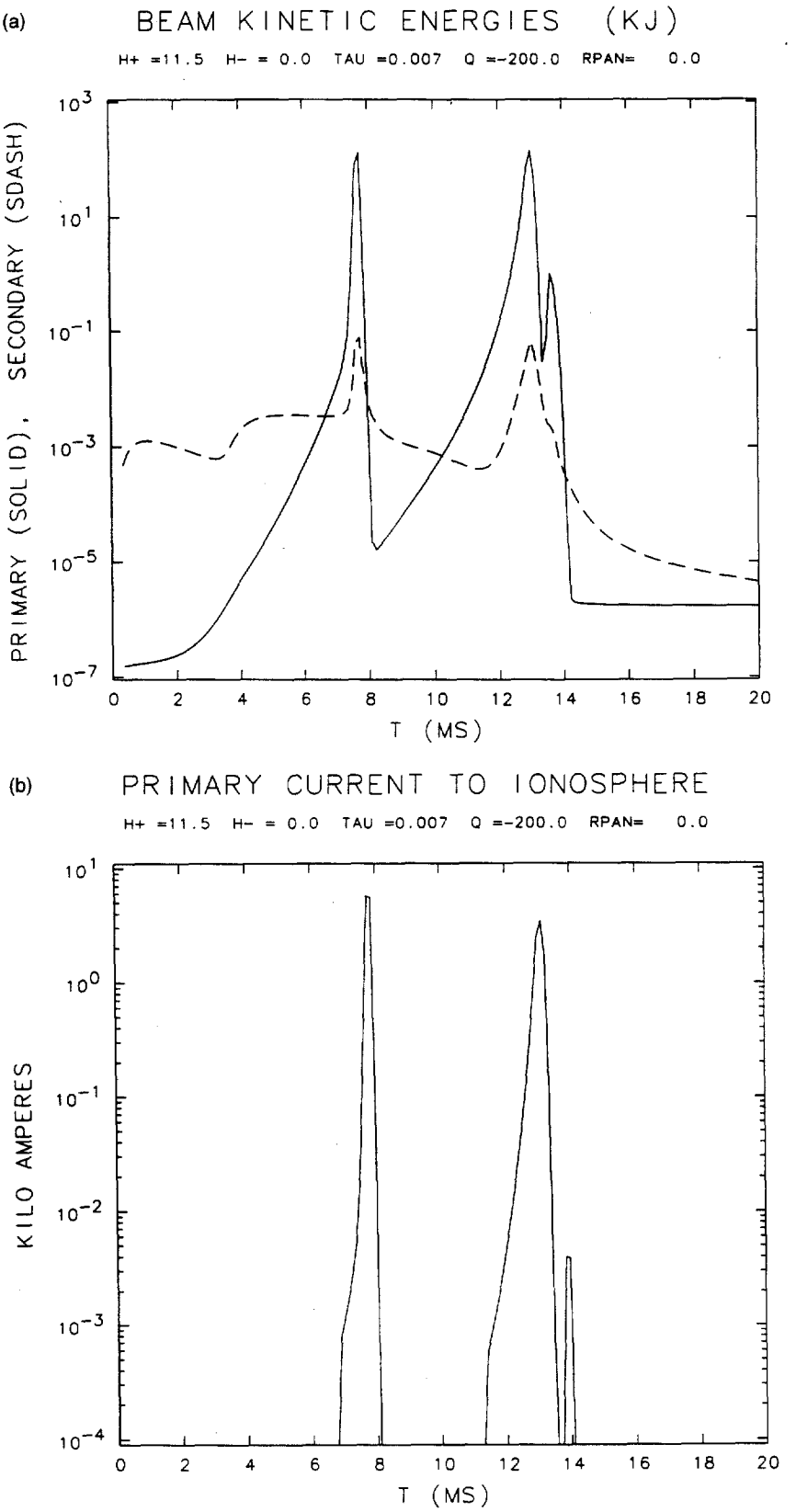

Fig. 5. Total beam and secondary electron kinetic energies and beam current. The primary and secondary electron kinetic energies (in kJ) integrated over the entire grid are plotted as a function of time in (a) for Case 2 (neutralization of 200 C at 11.5 km altitude in 7 ms). The corresponding primary electron current (in kA) leaving the top of the simulation grid for Case 2 is plotted as a function of time in (b).

Table 1
Selected simulation results

Case	τ (ms)	n_p (#/cc)	KE_p (kJ)	$I_{ionosphere}$ (kA)	E (V/m)	Airplane (kR)	Ground (kR)	γ (#/cm^2 s)
1	10	0.4	107	4.0	19	518	129	16800
2	7	0.5	144	5.7	37	647	162	17900
3	5	0.7	248	12	45	811	203	22500
4	3	1.2	376	19	75	1102	292	30500

population is 1000 times less than the primary beam, its dynamic range is much less than the primary beam, and it persists longer. The secondary electrons persist because they are moving much slower and remain in the discharge volume, because even weak avalanche regions act as a significant source of secondary electrons, and because the attachment rates are small compared to the duration of the discharge at altitudes above 40 km. Figure 5(b) displays the current to the ionosphere due to primary electrons for the same case. Numerically, we spatially integrate the flux of primary electrons across the top boundary and then differentiate, numerically, between computational time dumps. The three distinct flashes of the primary electron population are again seen in the currents, which reach several kA for a few tenths of a millisecond.

Table 1 summarizes some key outputs from the four sprite simulations. Recall that in each case 200 C was discharged at 11.5 km altitude, modeling a strong positive cloud-to-ground stroke. The tabulated outputs include the maximum primary electron number density (n_p); the maximum primary electron kinetic energy (KE_p); the maximum primary electron current to the ionosphere ($I_{ionosphere}$); the maximum radiation electric field strength (E); the maximum, first flash, visible intensity as seen from 11 km altitude (Airplane); the maximum, first flash, visible intensity as seen from the ground (Ground), and the maximum γ-flux (γ's). The visible emissions are calculated 300 km from the discharge center. The maximum radiating electric field is calculated 50 km from the discharge center (which is around 45 km altitude) and at an altitude of 80 km. The maximum γ-ray flux is calculated at 1000 km from the center of the discharge. The γ-ray flux is highly angular dependent and has a dynamic range of seven orders of magnitude over the range of observer positions relative to the vertical axis of the discharge.

We are presenting only the maximum visible intensities for the first flash because we are neglecting a significant emission process due to secondary electrons. The enhanced conductivity in the discharge region reduces the electric field below the threshold and the residual field maintains a low energy (~ 1 eV) population of secondary

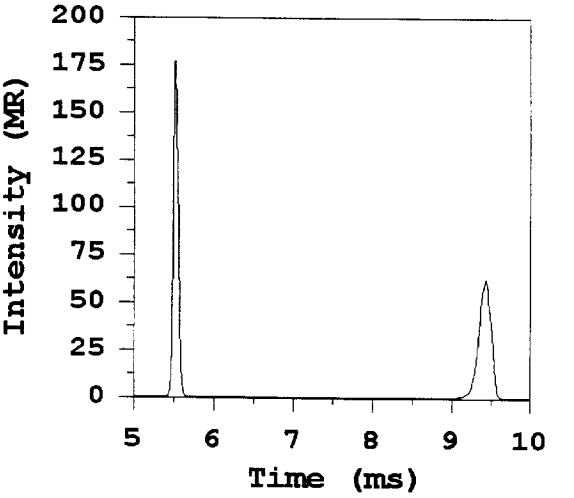

Fig. 6. Instantaneous optical intensity. The instantaneous optical intensity (in MR) at 51 km altitude is plotted as a function of time for Case 3 (neutralization of 200 C at 11.5 km altitude in 5 ms).

electrons which produces predominately red emissions. This process becomes important between flashes, i.e. when there are abundant secondary electrons but very few primary electrons left. In fact, the primary electron population drops by more than four orders of magnitude between flashes. Figure 6 plots the instantaneous visible intensity (note the short duration of these flashes), at 51 km altitude, as a function of time for case 3. At this altitude the first flash dominates and the third flash does not even develop. The neglected secondary electron emission process would contribute between 5.5 and 9 ms and after 9.5 ms when the primary electron population is negligible. We are therefore underestimating the optical emissions or, alternatively, we are overestimating the amount of charge needed in the normal lightning event to drive the red sprite formation. Finally, we find that all outputs increase with increasing case number or as the exponential neutralization time scale decreases. The vis-

ible emissions, radio output, and γ-ray flux are described in more detail in the next section.

3. Predicted emissions

We compute the spatial and temporal distribution of optical, radio and γ-ray emissions for each of the four cases discussed above. The results of the kinetic theory of runaway air breakdown (Roussel-Dupré et al., 1994) are used in our numerical calculations.

To calculate the optical emissions we use the air fluorescence efficiencies measured by Davidson and O'Neil (1964) and Mitchell (1970). Thus, given the spatial and temporal distribution of the number density and energy of primary electrons and integrating along the line of sight, it is possible to compute the corresponding distribution of optical emissions in space and time. We emphasize that the efficiencies used in our calculations are appropriate only for energetic particles in air without an applied electric field. The effect of the field is to maintain a population of secondary electrons at energies (~ 1 eV, for $\delta_0 = 1$) sufficient to cause additional excitation of the N_2 1st positive lines. Thus our results underestimate the red emissions and overestimate the charge neutralization needed to produce a discharge of this magnitude. Atmospheric attenuation from the source to the detector is incorporated in our calculations using the extinction coefficients measured by Guttman (1968).

The intensity of optical emissions averaged over 17 ms (corresponding to one camera frame) for the case when 200 C of charge is neutralized by a positive cloud-to-ground strike in 7 ms at an altitude of 11.5 km (case 2) is shown in Fig. 7(a). In this case the attenuation is calculated for a detector situated at an altitude of 11 km above sea level (corresponding to an aircraft) and the resulting image is shown on a true linear color scale. The maximum intensity is calculated to be 647 kR, while the spatial dimensions of the emitting region extend over 35 km $\times$ 30 km. The spectral intensity of the emission in the wavelength range from 400 to 900 nm as a function of altitude is shown in Fig. 7(c). Note that the red emissions resulting from the first positive band of nitrogen predominate at altitudes higher than 55 km, while at altitudes lower than 55 km the blue emissions resulting from the second positive and first negative bands of nitrogen predominate. Figure 7(b) shows optical emissions for the same discharge region as viewed from an altitude of 1 km above sea level (corresponding, for example, to the Yucca Ridge Field Station observing site in Colorado). The maximum intensity in this case is 162 kR. The spectral intensity viewed from this altitude is shown in Fig. 7(d). Our calculations show that the duration of the peak intensity of this simulated sprite is in the range from 0.3 to 3.5 ms, depending on altitude. At lower altitudes the duration of optical emissions is shorter than at higher altitudes.

The radio emissions produced by high-altitude discharges are computed using the space-time distribution of electrical current density and charged particle number density provided by the numerical simulations. The temporal evolution of the radiated electric field for an observer at an altitude of 80 km and a distance of 50 km from the center of the discharge is shown in Fig. 7(e) for case 2. The maximum electric field amplitude is 37 V/m. Our results show that radio emissions from sprite discharges can be comparable with those from regular lightning [see Uman (1984) for details] both in terms of amplitude (maximum values observed are about 50 V/m at an altitude of 80 km) and duration (in the range from 25 to 2000 μs for the case of a positive stroke). Therefore, it seems reasonable to conclude that ionospheric phenomena usually associated with radio emissions from a conventional lightning strike such as ionospheric heating and airglow, lower-hybrid wave generation, explosive spread F, and others can also be initiated by high-altitude discharges.

Given the velocity distribution and number density of relativistic electrons in space and time, we compute the corresponding spatial and temporal distribution of γ-rays generated by the discharge. In our calculations we employ the emissivities obtained by Roussel-Dupré et al. (1994) based on the Bethe–Heitler doubly differential cross section for bremsstrahlung emission by a relativistic electron. We consider γ-ray photons with energy $E > 30$ keV. The temporal evolution of the γ-ray flux seen by an observer at an altitude of 700 km and a distance from the center of the discharge of 1000 km is shown in Fig. 7(f) for case 2. The maximum value of the γ-ray flux is ~ 120 photons/cm^2·s while the duration of a single pulse is about 0.3 ms. The peak γ-ray flux angle distribution at a distance of 1000 km from the discharge center is shown in Fig. 7(g). The angle distribution is calculated without taking into account atmospheric absorption which for energies above 30 keV can only be neglected for a radiating source situated above 50 km altitude.

Figures 8(a) and (b) show the optical intensity for case 1 where 200 C of charge is neutralized by a positive cloud-to-ground strike in 10 ms at an altitude of 11.5 km as seen from altitudes of 11 km and 1 km above sea level respectively. The maximum optical intensities for these cases are 518 kR and 129 kR, respectively. The radiated electric field as a function of time for an observer at an altitude of 80 km and a distance from the center of the discharge of 50 km is shown in Fig. 8(c). The peak γ-ray flux angle distribution at a 1000 km distance from the discharge center is shown in Fig. 8(d).

Figures 9(a) and (b) show the optical intensity for case 3 where 200 C of charge is neutralized by a positive cloud-to-ground strike in 5 ms at an altitude of 11.5 km as seen from altitudes of 11 km and 1 km above sea level,

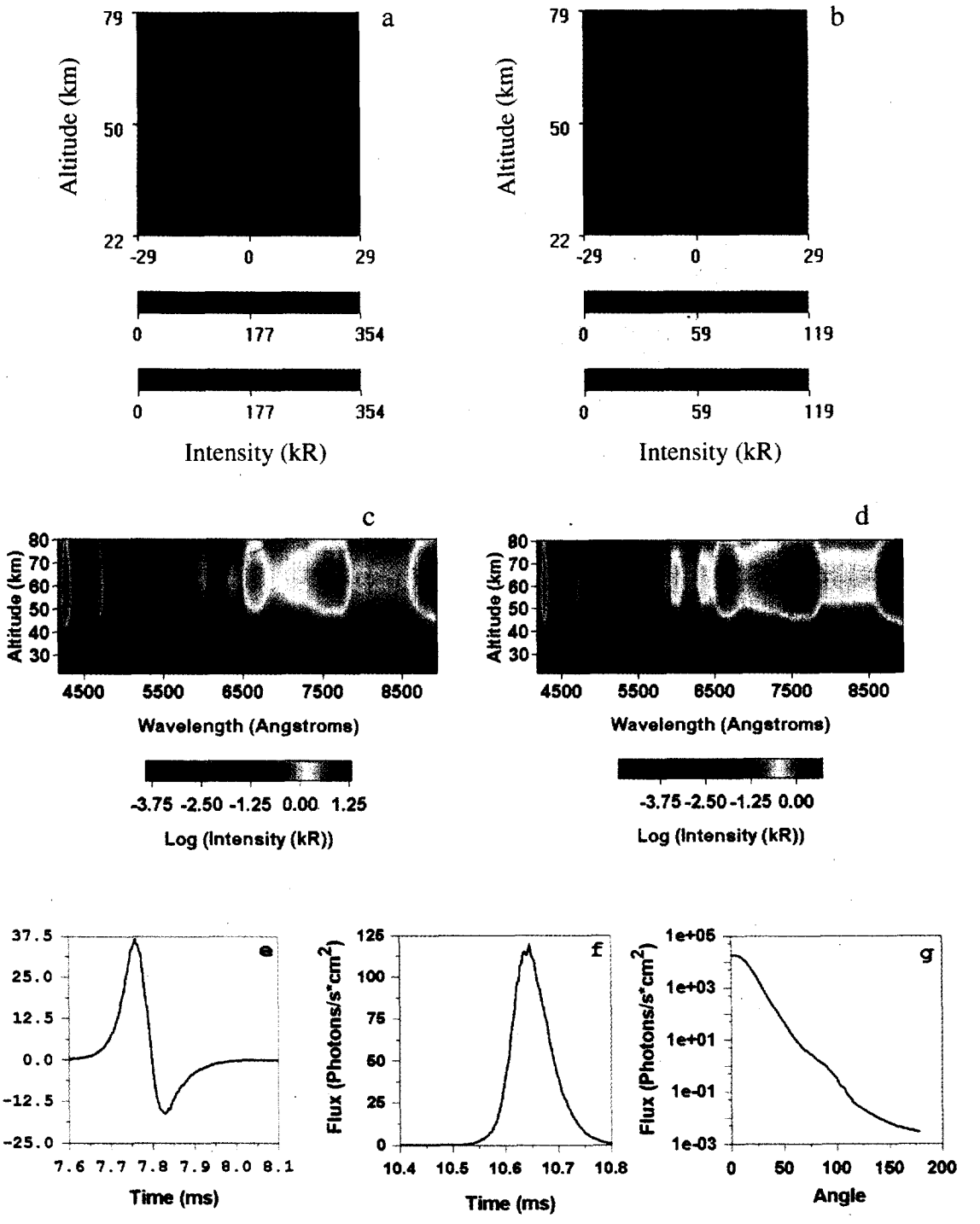

Fig. 7. Computed optical, radio frequency, and X- and γ-ray emissions for Case 2. The computed optical image averaged over 17 ms for a detector situated at an altitude of 11 km is presented in (a) for Case 2 (neutralization of 200 C at 11.5 km altitude in 7 ms) on a true linear color scale. The color bars give the intensity in kR. The corresponding image for a detector situated at an altitude of 1 km is shown in (b). The spectral intensity (kR) in the wavelength range from 400 to 900 nm and averaged over 17 ms is plotted as a function of height on a log color scale for a detector at an altitude of 11 km in (c). The corresponding spectra for a detector at 1 km altitude is shown in (d). The temporal evolution of the radiated electric field (in V/m) for an observer at an altitude of 80 km and a distance of 50 km from the center of the discharge is shown in (e). The temporal evolution of the X- and γ-ray flux (photons/cm^2·s) above 30 keV as seen by an observer at an altitude of 700 km and a distance from the center of the discharge of 1000 km is shown in (f). The peak X- and γ-ray flux (photons/cm^2·s) angle distribution at a distance of 1000 km from the discharge center is shown in (g).

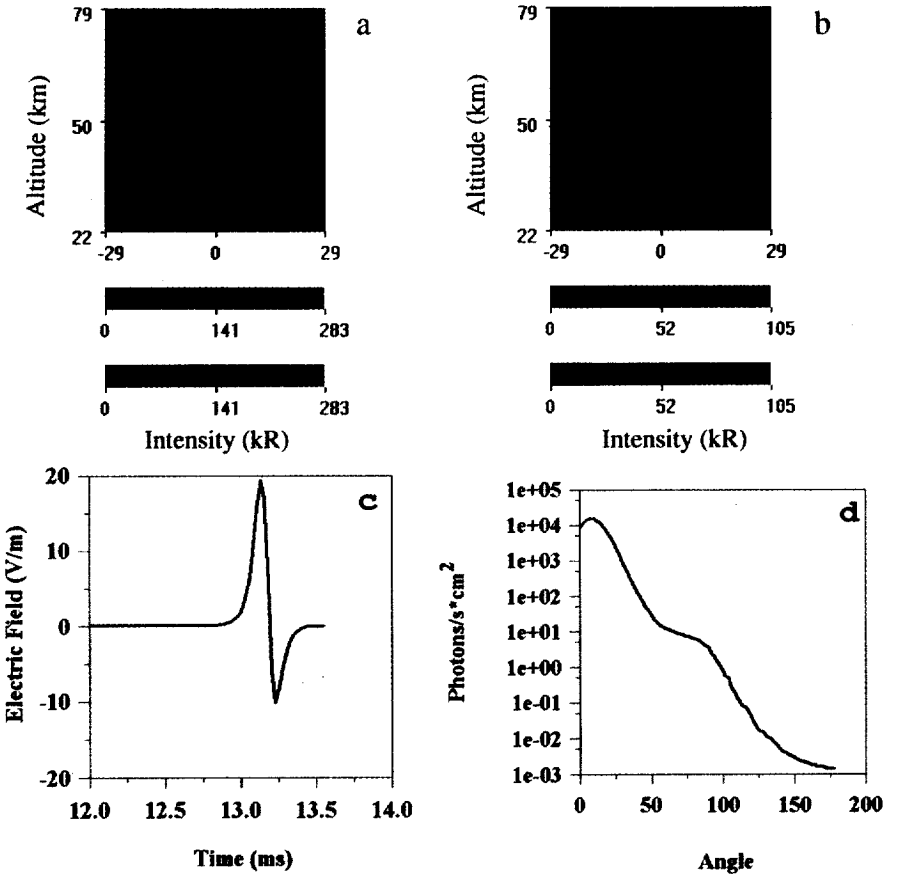

Fig. 8. Computed optical, radio frequency, and X- and γ-ray emissions for Case 1. The computed optical image averaged over 17 ms for a detector situated at an altitude of 11 km is presented in (a) for Case 1 (neutralization of 200 C at 11.5 km altitude in 10 ms) on a true linear color scale. The color bars give the intensity in kR. The corresponding image for a detector situated at an altitude of 1 km is shown in (b). The temporal evolution of the radiated electric field in (V/m) for an observer at an altitude of 80 km and a distance of 50 km from the center of the discharge is shown in (c). The peak X- and γ-ray flux (photons/cm^2·s) angle distribution at a distance of 1000 km from the discharge center is shown in (d).

respectively. The maximum optical intensities are 811 kR (view from 11 km) and 203 kR (view from 1 km). The radiated electric field as a function of time for an observer at an altitude of 80 km and a distance from the discharge center of 50 km is shown in Fig. 8(c) for this case. The γ-ray flux angle distribution at a 1000 km distance from the discharge center is shown in Fig. 8(d). Finally, we note that the optical, γ-ray, and radio emissions computed for case 4 are quite similar to those obtained for case 3.

4. Comparison with observations

The computed intensity of optical emissions for the case when the observer is at an altitude of 11 km above sea level [Figs 7(a), 8(a), 9(a)] is in excellent agreement with the results of aircraft observations (Sentman et al., 1995). The peak value of the intensity measured by Sentman et al. (1995) for the brightest sprite is about 600 kR, and is comparable to the computed value of 647 kR for case 2. Both the observational picture and the pictures [Figs 7(a)–9(a)] obtained from our simulations show the presence of blue emission at the bottom of the red sprite (blue tendrils), extending down to 40 km. The blue tendril is visible only from high altitudes ($h \sim 11$ km), and becomes invisible from low altitudes because of Rayleigh scattering and scattering from aerosols. This result is in agreement with certain ground-based observations of red sprites (Winckler et al., 1996; Rairden and Mende, 1995; Lyons, 1996), which show no evidence for blue tendrils. Recent ground-based observations of red sprites (Lyons, 1996) show sprite tops at an average altitude of 77 km and sprite bases at an average altitude of 50 km. As one can see in Figs 7(b), 8(b), and 9(b), which represent the

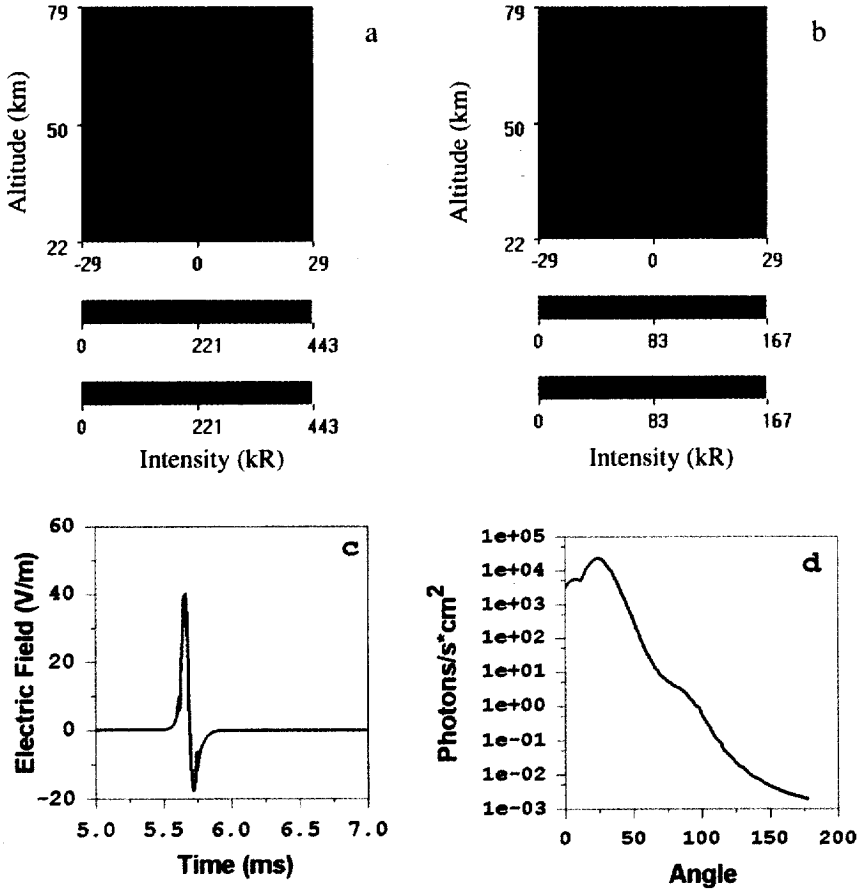

Fig. 9. Computed optical, radio frequency, and X- and γ-ray emissions for Case 3. The computed optical image averaged over 17 ms. for a detector situated at an altitude of 11 km is presented in (a) for Case 3 (neutralization of 200 C at 11.5 km altitude in 5 ms) on a true linear color scale. The color bars give the intensity in kR. The corresponding image for a detector situated at an altitude of 1 km is shown in (b). The temporal evolution of the radiated electric field (in V/m) for an observer at an altitude of 80 km and a distance of 50 km from the center of the discharge is shown in (c). The peak X- and γ-ray flux (photons/cm^2·s) angle distribution at a distance of 1000 km from the discharge center is shown in (d).

images of red sprites obtained assuming that the observer is at low altitude, our results are consistent with these observations.

The computed spectra of optical emissions are in agreement with observational data obtained by Hampton et al. (1996) in the wavelength range from 550 nm to 850 nm. Both the data and the calculations clearly show the dominance in sprite spectra of red emissions resulting from transitions in the 1st positive band of nitrogen. The lack of recorded spectra in the blue makes it impossible for us to compare our calculations with observations and is partially a result of the strong atmospheric attenuation that occurs over the long path lengths from source to detector, as demonstrated in the calculations. We also point out that our simulations indicate that the energetic part of the runaway discharge has a much shorter duration (a few ms) than the camera integration time (17 ms) and that a large component of the recorded spectra in the red could originate from additional excitation caused by a residual population of low energy ($\sim$1 eV) secondary electrons maintained by a persistent thunderstorm electric field that lies just below the threshold for runaway. The latter effect, which is not included in our simulations, will be the subject of future investigations. Thus while the camera sensitivity is able to register the much stronger and longer duration red component, it may not be sufficient to record the attenuated and shorter duration blue component. The duration of the peak intensity of optical emissions of sprites obtained from our calculations is in the range from 0.3 to 3.5 ms. These results are in agreement with the photometer measurements of Winckler et al. (1996), who show an average duration for sprites of about 3 ms. A more detailed description of the optical (including detailed

spectra with references to the N_2^+ 1st negative and Meinel bands and to the N_2 2nd positive band) emissions produced by runaway discharges appears in a companion paper (Yukhimuk et al., 1997).

The computed values for the γ-ray fluxes caused by upward propagating discharges are in agreement with observations of γ-ray bursts of atmospheric origin as reported by Fishman et al. (1994). The scintillation detectors used for the observations are sensitive to photons with energies above 20 keV; in our calculation we considered γ-ray photons with energy $£ > 30$ keV. As one can see from Fig. 7(g), the peak γ-ray flux depends significantly on the angle of observation. For an observer at approximately 90°, the computed flux is 0.25 photons/s·cm^2, while at approximately 0° the flux is larger than 10^4 photons/s·cm^2. The measurements of Fishman et al. (1994) yield a γ-ray flux of about 100 photons/s·cm^2. It should be noted that we calculate the γ-ray flux without taking into account atmospheric scattering and absorption. Scattering will lead to an increase in the duration of the pulse simultaneously with a decrease in the flux peak value. Our simulations show that upward discharges have a tendency to produce several short (with a duration of about 0.1–0.5 ms) γ-ray pulses with a time separation of about 01.–1 ms. Depending on the source altitude for a given event, multiple pulses of this type would become blended and yield an event composed of fewer individual peaks and with an extended duration as a result of scattering. Indeed, such a temporal structure was observed by Fishman et al. (1994) and γ-ray pulses with durations of about 1–3 ms usually possess multiple peaks.

A more detailed comparison of optical (including detailed spectra with references to the N_2^+ 1st negative and Meinel band emissions), radio, and γ-ray emissions produced by runaway discharges are being published in a companion paper (Yukhimuk et al., 1997).

5. Summary

Detailed 2D hydrodynamic and quasi-electrostatic simulations of high-altitude discharges driven by runaway air breakdown were presented for four cases corresponding to sprites initiated by positive cloud-to-ground lightning strikes in which 200 C of charge is neutralized at an altitude of 11.5 km in 10, 7, 5 and 3 ms. We find that the computed optical emissions agree well with low-light level camera images of sprites, both in terms of the overall intensity and spatial distribution of the emissions. The computed spectra in the wavelength range 550–850 nm are also in good agreement with observations as is the altitude (55 km) which marks the transition from the dominance of red emissions to that of blue emissions. The computed time dependence of the optical emissions is also in good agreement with observations and is characterized by several intensity peaks with durations ranging from several hundred μs to several ms. The simulations indicate that these peaks are associated with several discharge events.

When the driving quasi-electrostatic field exceeds the runaway threshold, it initiates a discharge that creates a highly conducting medium of finite spatial extent near the axis of the charge distribution in the cloud. The conductivity is sufficiently high to eliminate the field in this region rapidly; however, the field continues to grow on the edges (as the driving lightning discharge proceeds) and eventually exceeds the threshold on the edges. A runaway discharge then occurs in a region surrounding the initial core breakdown region. Meanwhile three-body attachment reduces the conductivity in the core and leads to recovery of the field and a second discharge is driven in the core region at lower altitudes. This basic cycle can be repeated several times depending on the duration and strength of the driving lightning discharge and results in several bursts of optical emissions. Following an initial discharge (or set of discharges) the conductivity relaxes back to the background value, and depending on the relaxation times and the evolution of the discharge, it is also possible for a residual electric field that is below the threshold for runaway to persist for long periods of time. This field can maintain a low energy (~ 1 eV) population of secondary electrons which would predominately produce red emissions. Thus we would expect to see rapid (a few ms) emissions across the visible spectrum followed by a persistent (several hundred ms) red component. Indeed the observations support this picture (see Winckler et al., 1996); it is also not surprising that red emissions would dominate when integrated over a camera frame. We note that the peak secondary electron densities ($\sim 5 \times 10^{10}$ m^3) obtained in our simulations as well as their lifetimes (several hundred ms) are in good agreement with recent measurements of RF echoes associated with lightning (see Roussel-Dupré and Blanc, 1997).

All four cases considered in this paper have yielded strong radio pulses with durations of ~ 300 μs and peak electric field amplitudes ranging from 20 to 75 V/m at an altitude of 80 km and an approximate distance of 50 km. The magnitude and duration of these pulses is sufficient to cause breakdown and heating of the lower ionosphere (80–95 km) and leads us to suggest that sprites may also launch the EMP responsible for the production of elves. This subject will be discussed in more detail in a future publication. We note that these particular simulations did not produce pairs of pulses that resembled the measured transionospheric pulse pairs (TIPPs, see Holden et al., 1995) as suggested by Roussel-Dupré and Gurevich (1996); however, the latter calculations did not allow for the self-consistent annihilation of the field due to the enhanced conductivity created by the discharge. On the basis of the discharge characteristics and the computed pulses we conclude that faster initiating lightning discharges than those considered here and by Roussel-

Dupré and Gurevich would be required. These discharges in turn may not produce sufficient optical emissions (when integrated over a camera frame) to be observed. In this case, TIPPs may not be associated with observable sprites but could still be produced by high-altitude discharges. The relation of TIPPs to high-altitude discharges is presently under investigation.

The γ-ray bursts of atmospheric origin reported by Fishman et al. (1994) can only arise from a source situated at an altitude above 25 km in the atmosphere. Therefore it seems only natural to associate these measurements with high-altitude discharges. Our sprite simulations yield results in good agreement with both the amplitude and the temporal signature of the measured γ- and X-ray fluxes above 30 keV.

The bremsstrahlung emissions produced by the electron beam in a runaway discharge is a unique signature of this mechanism and there is mounting evidence to suggest that runaway breakdown is at work not only at high-altitudes (e.g. sprites) but also in the discharges and overall electrical activity occurring within and below thunderstorms. A high-altitude experiment in which a balloon platform is outfitted with appropriate optical and X- and γ-ray diagnostics and is directed over a mesoscale convective system at an altitude of $\sim$25 km could provide final confirmation for the role of runaway processes in producing sprites and other high-altitude discharges.

Acknowledgements

This work was funded by NASA grant NRA-95-11-ITM-29 and supported in part by the DoE and Air Force contracts N000CZ73700111 and N000CZ73700109.

References

Addessio, F.L., Baumgardner, J.R., Dukowicz, J.K., Johnson, N.L., Kashiwa, B.A., Rauenzahn, R.M., Zemach, C., 1992. CAVEAT: A computer code for fluid dynamics problems with large distortion and internal slip. Los Alamos National Laboratory Report LA-10613-MS, Rev. 1.

Ali, A.W., 1986. Intense and short electric field (dc and microwave) air-breakdown parameters. NRL Memorandum Report, p. 5815.

Armstrong, R.A., Shorter, J.A., Lyons, W.A., Jeong, L.S., Blumberg, W.A.M., 1996. Photometric measurements in the SPRITES '95 campaign: Evidence for nitrogen first negative (4278A) emission. Preprint.

Bell, T.F., Pasko, V.P., Inan, U.S., 1995. Runaway electrons as a source of red sprites in the mesosphere. Geophys. Res. Lett. 22, 2127.

Bethe, H.A., 1930. Theory of passage of swift corpuscular rays through matter. Ann. Phys. 5, 325.

Bethe, H.A., Ashkin, J., 1953. Penetration of beta-rays through matter. In Segre, E., Ed. Experimental Nuclear Physics. John Wiley and Sons, New York, p. 277.

Boccippio, D.J., Williams, E.R., Heckman, S.J., Lyons, W.A., Baker, I.T., Boldi, R., 1995. Sprites, ELF transients, and positive ground strokes. Science 269, 1088.

Boeck, W.L., Vaughan, Jr., O.H., Blakeslee, R.J., 1990. Low light level television images of terrestrial lightning as viewed from space. EOS Trans. AGU 72, 171.

Boeck, W.L., Vaughan, Jr., O.H., Blakeslee, R.J., Vonnegut, B., Brook, M., McKune, J., 1995. Observations of lightning in the stratosphere. J. Geophys. Res. 100, 1465.

Davidson, G., O'Neil, R., 1964. Optical radiation from nitrogen and air at high pressure excited by energetic electrons. J. Chem. Phys. 41, 3946.

Daniel, R.R., Stephens, S.A., 1974. Cosmic-ray-produced electrons and gamma rays in the atmosphere. Rev. Geophys. Spa. Phys. 12, 233.

Eack, K.B., Beasley, W.H., Rust, W.D., Marshall, T.C., Stolzenburg, M., 1996. X-ray pulses observed above a mesoscale convective system. Geophys. Res. Lett. 23, 2915.

Fishman, G.J., Bhat, P.N., Mallozzi, R., Horack, J.M., Koshut, T., Kouveliotou, C., Pendleton, G.N., Meegan, C.A., Wilson, R.B., Paciesas, W.S., Goodman, S.J., Christian, H.J., 1994. Discovery of intense gamma-ray flashes of atmospheric origin. Science 264, 1313.

Franz, R.C., Nemzek, R.J., Winckler, J.R., 1990. Television image of a large upward electrical discharge above a thunderstorm system. Science 249, 48.

Fukunishi, H., Takahashi, Y., Kubota, M., Sakanoi, K., Inan, U.S., Lyons, W.A., 1996. Elves: Lightning-induced transient luminous events in the lower ionosphere. Geophys. Res. Lett. 23, 2157.

Glukhov, V.S., Inan, U.S., 1996. Particle simulation of the time-dependent interaction with the ionosphere of rapidly varying lightning EMP. Geophys. Res. Lett. 23, 2193.

Gurevich, A.V., Milikh, G.M., Roussel-Dupré, R.A., 1992. Runaway electron mechanism of air breakdown and preconditioning during a thunderstorm. Phys. Lett. A 165, 463.

Gurevich, A.V., Milikh, G.M., Roussel-Dupré, R.A., 1994. Nonuniform runaway air-breakdown. Phys. Lett. A 187, 197.

Guttman, A., 1968. Extinction coefficient measurements on clear atmospheres and thin cirrus clouds. Appl. Opt. 7, 2377.

Hampton, D.L., Heavner, M.J., Wescott, E.M., Sentman, D.D., 1996. Optical spectral characteristics of sprites. Geophys. Res. Lett. 23, 89.

Holden, D.N., Munson, C.P., Devenport, J.C., 1995. Satellite observations of transionospheric pulse pairs. Geophys. Res. Lett. 22, 889.

Huxley, L.G.H., Crompton, R.W., 1974. The diffusion and drift of electrons in gases. Wiley Series in Plasma Physics. John Wiley & Sons, New York.

Inan, U.S., Bell, T.F., Rodriguez, J.V., 1991. Heating and ionization of the lower ionosphere by lightning. Geophys. Res. Lett. 18, 705.

Inan, U.S., Bell, T.F., Pasko, V.P., Sentman, D.D., Wescott, E.M., Lyons, W.A., 1995. VLF signatures of ionospheric disturbances associated with sprites. Geophys. Res. Lett. 22, 3461.

Inan, U.S., Sampson, W.A., Taranenko, Y.N., 1996. Space-time structure of optical flashes and ionization changes produced by lightning-EMP. Geophys. Res. Lett. 23, 133.

Lyons, W.A., Williams, E.R., 1993. Preliminary investigations of the phenomenology of cloud-to-stratospheric lightning discharges. 17th Conference on Severe Local Storms/Conference on Atmospheric Electricity, American Meteorological Society, St. Louis MO.

Lyons, W.A., 1994. Characteristics of luminous structures in the stratosphere above thunderstorms as imaged by low-light video. Geophys. Res. Lett. 21, 875.

Lyons, W.A., Winckler, J.R., Nemzek, R.J., Malcolm, P.R., Williams, E.R., Boccippio, D., 1994. The 1994 Colorado SPRITE Campaign: Initial Results. EOS Transactions of the AGU 1994 Fall Meeting 75, (44), 108.

Lyons, W.A., 1996. Sprite observations above the U.S. High Plains in relation to their parent thunderstorm systems. J. Geophys. Res. 101, 29641.

McCarthy, M.P., Parks, G.K., 1985. Further Observations of X-rays inside thunderstorms. Geophys. Res. Lett. 12, 393.

Mende, S.B., Rairden, R.L., Swenson, G.R., Lyons, W.A., 1995. Sprite spectra; N_2 1 PG band identification. Geophys. Res. Lett. 22, 2633.

Milikh, G.M., Papadopoulos, K., Chang, C.L., 1995. On the physics of high altitude lightning. Geophys. Res. Lett. 22, 85.

Mitchell, K.B., 1970. Fluorescence efficiencies and collisional deactivation rates for N_2 and N_2^- bands excited by soft X-rays. J. Chem. Phys. 53, 1795.

Parks, G.K., Mauk, B.H., Spiger, R., Chin, J., 1981. X-ray enhancements detected during thunderstorm and lightning activities. Geophys. Res. Lett. 8, 1176.

Pasko, V.P., Inan, U.S., Taranenko, Y.N., Bell, T.F., 1995. Heating, ionization, and upward discharges in the mesosphere due to intense quasi-electrostatic thundercloud fields. Geophys. Res. Lett. 22, 365.

Pasko, V.P., Inan, U.S., Bell, T.F., 1996. Sprites as luminous columns of ionization produced by quasi-electrostatic thundercloud fields. Geophys. Res. Lett. 23, 649.

Piper, L., Green, D., Blumberg, W.A.M., Wolnik, S., 1985. N_2^+ Meinel band quenching. J. Chem. Phys. 82, 3139.

Rairden, R.L., Mende, S.B., 1995. Time resolved sprite imagery. Geophys. Res. Lett. 22, 3465.

Roussel-Dupré, R.A., Gurevich, A.V., Tunnell, T., Milikh, G.M., 1994. Kinetic theory of runaway air breakdown. Phys. Rev. E 49, 2257.

Roussel-Dupré, R.A., Gurevich, A.V., 1996. On runaway breakdown and upward propagating discharges. J. Geophys. Res. 101, 2297.

Roussel-Dupré, R.A., Blanc, E., 1997. HF echoes from ionization potentially produced by high-altitude discharges. J. Geophys. Res. 102, 148.

Rowland, H.L., Fernsler, R.F., Huba, J.D., Bernhardt, P.A., 1995. Lightning driven EMP in the upper atmosphere. Geophys. Res. Lett. 22, (4), 361.

Sentman, D.D., Westcott, E.M., 1993. Observations of upper atmospheric optical flashes recorded from an aircraft. Geophys. Res. Lett. 20, 2857.

Sentman, D.D., Wescott, E.M., Osborne, D.L., Hampton, D.L., Heavner, M.J., 1995. Preliminary results from the Sprites '94 aircraft campaign: 1. Red sprites. Geophys. Res. Lett. 22, 1205.

Sukhorukov, A. I., Rudenchik, E.A., Stubbe, P., 1996. Simulation of the strong lightning pulse penetration into the lower ionosphere. Geophys. Res. Lett. 23, (21), 2911.

Suszcynsky, D.M., Roussel-Dupré, R., DeHaven, H., Symbalisty, E., Voss, S., 1996. Blue-light imagery and photometry of sprites. EOS Transactions of the AGU 77, (46), F69.

Taranenko, Y.N., Inan, U.S., Bell, T.F., 1993a. Interaction with the lower ionosphere of electromagnetic pulses from lightning: Heating, attachment and ionization. Geophys. Res. Lett. 20, 1539.

Taranenko, Y.N., Inan, U.S., Bell, T.F., 1993b. Interaction with the lower ionosphere of electromagnetic pulses from lightning: excitation of optical emissions. Geophys. Res. Lett. 20, 2675.

Taranenko, Y.N., Roussel-Dupré, R., 1996. High-altitude discharges and gamma-ray flashes: A manifestation of runaway air breakdown. Geophys. Res. Lett. 23, 571.

Taranenko, Y.N., Roussel-Dupré, R., 1997. Response to comments by K. Papadopoulos and J.A. Valdivia. Geophys. Res. Lett. in press.

Uman, M.A., 1984. Lightning. Dover Publications, New York.

Vaughan, Jr., O.H., Blakeslee, R.J., Boeck, W.L., Vonnegut, B., Brook, M., McKune, Jr., J., 1992. A cloud-to-space lightning as recorded by the space shuttle payload-bay TV cameras. Monthly Weather Review 120, 1459.

Wescott, E.M., Sentman, D.D., Osborne, D.L., Hampton, D.L., Heavner, M.J., 1995. Preliminary results from the Sprites '94 aircraft campaign: 2. Blue jets. Geophys. Res. Lett. 22, 1209.

Wilson, C.T.R., 1925. The electric field of a thundercloud and some of its effects. Proceedings Royal Society, London 37, 32D.

Wilson, C.T.R., 1956. A theory of thundercloud electricity. Proceedings Royal Society, London 236, 297.

Winckler, J.R., Franz, R.C., Nemzek, R.J., 1993. Fast low-level light pulses from the night sky observed with the SKYFLASH Program. J. Geophys. Res. 98, 8775.

Winckler, J.R., Lyons, W.A., Nemzek, R.J., 1994. New high-resolution ground-based studies of cloud-ionosphere discharges (CI's). EOS Transactions of the AGU 1994 Fall Meeting 75, (44), 107.

Winckler, J.R., Lyons, W.A., Nelson, T.E., Nemzek, R.J., 1996. New high-resolution ground-based studies of sprites. J. Geophys. Res. 101, 6997.

Yukhimuk, V., Roussel-Dupré, R., Taranenko, Y., E.M.D., 1997. Symbalisty. Optical characteristics of red sprites produced by runaway air breakdown. J. Geophys. Res. in press.